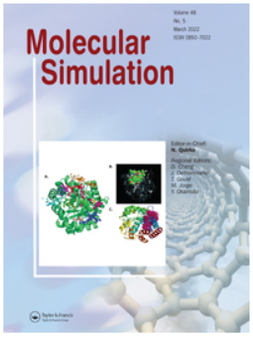

Molecular Simulation

ISSN: (Print) (Online) Journal homepage: https://www.tandfonline.com/loi/gmos20

Porous material adsorbents ZIF-8, ZIF-67, Co/Zn-ZIF and MIL-127(Fe) for separation of H_2S from an H_2S/CH_4 mixture

Tanawut Ploymeerusmee, Wolfhard Janke, Tawun Remsungnen, Supot Hannongbua & Tatiya Chokbunpiam

To cite this article: Tanawut Ploymeerusmee, Wolfhard Janke, Tawun Remsungnen, Supot Hannongbua & Tatiya Chokbunpiam (2022) Porous material adsorbents ZIF-8, ZIF-67, Co/Zn-ZIF and MIL-127(Fe) for separation of H_2S from an H_2S/CH_4 mixture, Molecular Simulation, 48:5, 417-426, DOI: 10.1080/08927022.2021.2025232

To link to this article: https://doi.org/10.1080/08927022.2021.2025232

MOLECULAR SIMULATION
2022, VOL. 48, NO. 5, 417–426
https://doi.org/10.1080/08927022.2021.2025232

Taylor & Francis
Taylor & Francis Group

Porous material adsorbents ZIF-8, ZIF-67, Co/Zn-ZIF and MIL-127(Fe) for separation of H_2S from an H_2S/CH_4 mixture

Tanawut Ploymeerusmee[a], Wolfhard Janke[b], Tawun Remsungnen[c], Supot Hannongbua[d] and Tatiya Chokbunpiam[e]

[a]Petrochemistry and Polymer Sciences Program, Faculty of Science, Chulalongkorn University, Bangkok, Thailand; [b]Faculty of Physics and Geosciences, Institute of Theoretical Physics, University of Leipzig, Leipzig, Germany; [c]Faculty of Applied Science and Engineering, Khon Kaen University, Nong Khai, Thailand; [d]Computational Chemistry Unit Cell, Department of Chemistry, Faculty of Science, Chulalongkorn University, Bangkok, Thailand; [e]Department of Chemistry, Faculty of Science, Ramkhamhaeng University, Bangkok, Thailand

ABSTRACT

The application of several porous solids for the purification of methane, representing natural gas, from H_2S is studied. Computer simulations yield adsorption isotherms and separation selectivity. All investigated materials are suited for the separation, but with different efficiency. For MIL-127(Fe) the selectivity CH_4/H_2S reaches values of about 250 at 2 bar and 250 K. The results can be initially concluded that the potential energy of each gas/material pair, free space inside the material and metal oxide are important keys for adsorption and separation of H_2S from CH_4.

ARTICLE HISTORY
Received 19 April 2021
Accepted 15 December 2021

KEYWORDS
Gibbs-Ensemble Monte-Carlo (GEMC) simulations; porous materials; natural gas

1. Introduction

Global energy consumption is increasing year by year [1–7]. There are two main categories of energy: non-renewable and renewable. The non-renewable energy resources are fossil fuels such as coal, natural gas and oil that are available in limited amounts because they take millions of years to replenish. Moreover, and more important at present, they produce a lot of CO_2 and other harmful gases when burned. On the other hand, renewable energies including solar, hydro and wind energy are principally unlimited because they replenish themselves. However, the availability of renewable energy at any given moment is limited and their storage is expensive and needs huge devices as barrier lakes or collections of batteries. Batteries have limited capacity and lifetime and their production is not eco-friendly. Particularly for transport of persons and goods, the operating distance of electro cars is quite short, and the batteries need, frequently, a long time to be re-loaded. Therefore, some kinds of non-renewable energy still are the main energy source [8–13].

The carbon (C) and hydrogen (H) content of the fuel essentially determines the amount of produced energy. When C and H combine with oxygen (O) during combustion, then heat is generated. The US Energy Information Administration [14] reported that natural gas combustion released around 50–60% less carbon dioxide than coal or oil. The emissions of carbon dioxide per million British thermal units (Btu) for various fuels are the following: coal (anthracite) 228.6 pounds, coal (bituminous) 205.7 pounds, coal (lignite) 215.4 pounds, coal (subbituminous) 214.3 pounds, diesel fuel and heating oil 161.3 pounds, gasoline 157.2 pounds, propane 139.0 pounds and natural gas 117.0 pounds. Natural gas is the cleanest source among the fossils because it has the lowest carbon content.

The major component of natural gas is methane, which has higher energy content relative to other fuels, and hence, it produces less carbon dioxide to energy content. Thus natural gas is cleaner than coal and reduces climate change [15]. Water and other elements, i.e. sulphur and noncombustible elements in some fuels, decrease their heating values and rise their carbon dioxide to heat contents.

Natural gas is used in several applications such as in industrial manufacturing, in residential heating or cooling, electric power, commercial and vehicle fuel. It consists of a hydrocarbon mixture (i.e. methane, ethane, propane, etc.). It contains also non-hydrogen compounds and various impurities. One important impurity in natural gas is hydrogen sulphide (H_2S), which needs to be removed before the gas is suitable for use. Sour gas or acid gas is a common name for natural gas that contains a significant amount of H_2S [16,17]. The H_2S forms a problematic compound for the gas industry because of toxicity, corrosion of devices and reduced efficiency of equipment, irritating odour, decreased value of products, and expanded operation costs. Therefore, H_2S elimination is a significant problem for the natural gas treatment process [18–23]. The natural gas treatment process includes different techniques [24–35]. (i) Physical absorption that relies on physical solvents, e.g. dimethyl ethers of polyethylene glycol (DEPG) shows no reaction between solvent and sour gas via counterflow. In this process, it is sometimes required to decrease the operating temperature to rise sour gas solubility and to reduce the solvent circulation rate. (ii) Chemical absorption involves the formation of reversible chemical bonds between the sour gas and the base solvent such as monoethanolamide (MEA), diethanolamine (DEA), diglycolamine (DGA) and sodium hydroxide (NaOH). In the process,

CONTACT Tatiya Chokbunpiam tatiya@ru.ac.th
Supplemental data for this article can be accessed online at https://doi.org/10.1080/08927022.2021.2025232.

the solvent itself undergoes regeneration, which involves bond breaking. The chemical solvent is good for removing sour gas but still has a problem with the separation of by-products from the solution, i.e. salt. (iii) Adsorption processes that use solid adsorbents such as activated carbon. The activated carbon is impregnated with alkaline solutions, such as sodium hydroxide (NaOH), potassium hydroxide (KOH), and potassium carbonate (K_2CO_3). Potassium carbonate was proven to be the best alkaline-impregnated activated carbon for effective adsorption capacity. However, disadvantages are the need of chemical inputs and the high cost of activated carbon via alkaline solutions. (iv) Use of granulates of solids that adsorb impurities, e.g. metal oxides or molecular sieves like zeolites or Metal-Organic Frameworks (MOFs). (v) Capillary condensation [33]. (vi) Use of membranes that act as molecular sieves. The gas is adsorbed at the membrane surface and it diffuses through barriers where some of the gases can move through the membrane more easily whereas other gases cannot pass or can pass in a lower amount. Membrane research for eliminating hydrogen sulphide requires many parameters to study such as pressure, temperature, concentration of the permeants and types of membrane [36]. For the separation of components, the permeability is ruled by selectivity (selectivity coefficient, separation coefficient).

Based on the information above, such techniques have attracted the attention of many scientists for reviewing and discussing, different processes. All have advantages and disadvantages. These must be investigated to increase efficiency and reduce the cost of separation procedures. The adsorption and membrane flow processes by porous materials seem to be very promising for the elimination of hydrogen sulphide from methane. The efficiency of porous materials depends on the surface area, porosity, specific function group of adsorbent, and upon the temperature, pressure and concentration of hydrogen sulphide. The separation of components of gas mixtures using porous materials was already investigated in several experimental and simulation studies [37–41]. The separation has been examined under the influence of an additional chemical reaction [42]. Several materials have extensively attracted scientists for studied the separation of H_2S/CH_4 mixture, for instance, UiO-66(Zr) [43], MIL [44,45], zeolite [46] and molecular sieves [47] which be the candidate materials in this field.

The objective of this work is to compare the separation of the H_2S impurity from methane if some porous materials are in use. We consider Zeolitic Imidazolate Frameworks (ZIFs), i.e. ZIF-8, ZIF-67, Co/Zn-ZIF and a MOF, namely, Materials of Institute Lavoisier-127 (MIL-127(Fe)). ZIF-8 has been chosen because it is one of the most common MOFs and one of the few MOFs that are already commercially produced and sold. Thus it may be of considerable interest to find out its performance for important technical processes. ZIF-67 and Co/Zn-ZIF are modifications of ZIF-8 and it is of scientific but also of practical interest if such modifications improve its performance for our purpose. As a contrast to this structure, we have additionally examined MIL-127(Fe) which showed good separation performance in earlier investigations of our group. This may help to decide if the ZIF-8 like structures are really optimal.

We try to achieve a better understanding of the mechanisms and the behaviour of the gases during these processes on a molecular scale. Moreover, the study should help to find optimal porous materials for the separation of the hydrogen sulphide impurity from methane.

2. Simulation methods

2.1. Investigation of adsorption

2.1.1. Gibbs-Ensemble Monte-Carlo (GEMC) simulations

All adsorption isotherms and adsorption selectivities (CH_4/H_2S) in the porous materials examined in this work are calculated in Gibbs Ensemble Monte Carlo (GEMC) simulations by use of the homemade Gibbon software, that has been used successfully in several papers including [42,48–53]. The main feature of this GEMC simulation method [54–57] is that the equilibrium between a gas phase and an adsorbed phase is being investigated directly, hence the input of fugacities from an empirical equation of state is not necessary. If GCMC is used, these fugacities are often calculated by the empirical Peng-Robinson equation of state [58]. For mixtures, this equation of state requires cross correction coefficients that are difficult to find in the literature and that, therefore are neglected in many cases. For moderate pressures and small molecules, this may be a reasonable approximation. We prefer to do the simulations without the use of an additional empirical equation and without neglecting cross corrections. However, a comparison of both methods (see the Supporting Material) shows that the results of both methods for the present system agree quite well.

In GEMC, the system consists of two simulation boxes. The first box (box A), contains the bulk gas mixture while the second box (box B), contains the porous framework and adsorbed guest molecules. The temperature, which is an input quantity in MC, is equal in both boxes. Metropolis MC translational and rotational moves are performed within both simulation boxes. Additionally, the molecules can be swapped between the two boxes, fulfilling the condition of microscopic reversibility following the algorithm of Rull et al. [59]. Such a swap move includes the removal of a molecule in one box and simultaneous insertion of that molecule in the other box. For details, see the Supporting Material.

The particle exchanges lead to equilibrium between the gas phase and the adsorbed phase. The GEMC simulation does not require knowledge of pressure or chemical potential. Instead, the state of the gas box is determined by the temperature and n particle densities. Thus $(n+1)$ intensive variables determine the gas phase in agreement with Gibbs rule. The state of the adsorbed phase is determined by the condition of equilibrium with the gas phase. But the pressure can be evaluated additionally if wished. This is desirable to compare the adsorption isotherms with experiments because the particle densities in the gas box are commonly not used (although known) for the abscissa in the presentation of adsorption isotherms by experimentalists or by engineers.

2.1.2 The adsorption isotherms

The size of box B was constant during each simulation run in this work corresponding to the rigid porous solid ($4 \times 4 \times 4$ unit cells), while the size of box A was varied to adjust to a

wished ideal gas pressure. Note that the simulation uses only particle densities and the pressures are only used for the presentation of results. For the final curves, the corresponding real gas pressure was calculated by use of the Peng–Robinson equation [58]. Details are explained in the Supporting Material.

Output quantities are the particle numbers in the gas phase and in the adsorbed phase in equilibrium. In this work, adsorption for the mixture CH_4/H_2S in porous materials is studied at 250 and 300 K and at pressures from 0.1 bar or 0.5 bar up to 20 bar.

For a better understanding of the high selectivity at 250 K, also the enthalpy of adsorption ΔH is evaluated at 250 K for both sorts at low pressure at which the differences in the adsorption behaviour of the two kinds of molecules become particularly clear. For rigid molecules and rigid lattice, at low density, according to [57,60] the enthalpy of adsorption is

W_{gh} is the sum of all potential guest–host energies. In the low-pressure region, where the average of the guest–host interaction energy of a given sort W_{gh} is a linear function of the number N_a of adsorbed molecules this becomes $\Delta H = <U_{gh}> - RT$, where $<U_{gh}>$ is the average guest host potential energy per particle and R is the universal gas constant. T is the temperature.

2.1.3 Adsorption selectivity

If the adsorption behaviour of two gas components i and j of a mixture are different, then the adsorption selectivity can be defined by the following equation [61]:

$N_{i,\text{adsorbed}}$ and $N_{j,\text{adsorbed}}$ are the numbers of adsorbed molecules of type i or j, respectively, in the porous material (box B). $N_{i,\text{ gas}}$ and $N_{j,\text{ gas}}$ are the numbers of molecules of type i or j, respectively in the gas phase (box A). In the present case, the CH_4 is sort i and H_2S is sort j.

In this work, in the gas phase (box A), the number of H_2S molecules was 5% of all molecules, and that of CH_4 molecules was 95% like typically in natural gas [17,62]. The adsorption selectivity of CH_4/H_2S in porous materials was examined at temperatures of 250 and 300 K and pressures between less than 1 bar (0.1 bar or 0.5 bar depending upon the system) and 20 bar.

2.2 Computational details

ZIF-8, ZIF-67, Co/Zn-ZIF and MIL-127(Fe) models are constructed from the XRD data of the Cambridge Crystallographic Data Center (CCDC) [63–66]. The cubic frameworks of ZIF-8, ZIF-67, Co/Zn-ZIF and MIL-127(Fe) for simulations consist of $4 \times 4 \times 4$ unit cells which have the corresponding lattice constants (unit cell edge lengths) of 16.9910 Å, 16.9589 Å, 17.099 Å and 21.985 Å, respectively. The structures are illustrated in Figure 1 and structural characteristics are in Supporting Material.

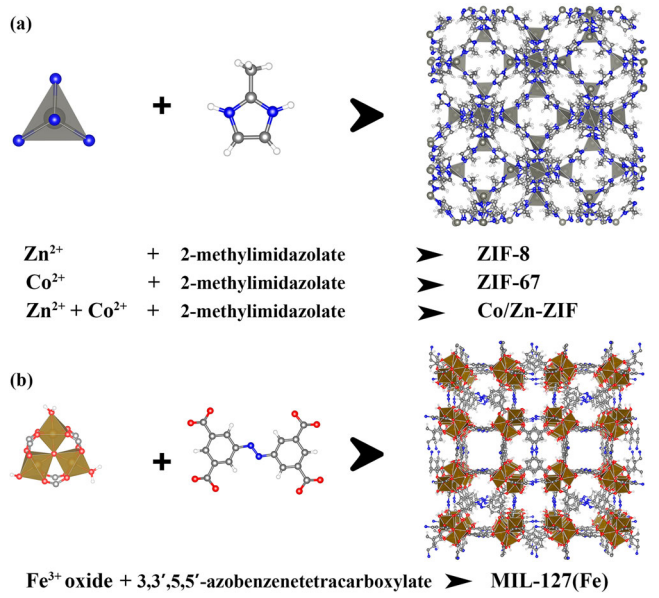

Figure 1. (Colour online) Lattice structure of (a) ZIF-8, ZIF-67 and Co/Zn-ZIF, (b) MIL-127(Fe) crystals.

In this work, the GEMC simulations have been done with rigid frameworks, which would not be possible for MD simulation of the diffusion of methane in ZIF-8, ZIF-90 and Co/Zn-ZIF. The diffusion selectivity depends strongly upon fluctuations of channel and aperture sizes in flexible frameworks. For example, for the separation of H_2/CH_4, the flexibility of the ZIF-8 framework changed the membrane selectivity by orders of magnitude because CH_4 diffusion in the rigid framework is much smaller than in the flexible one [38]. The reason is that the size of the methane molecule is not very different from the size of the windows connecting adjacent cavities. The influence of the flexibility on adsorption is much smaller because the fluctuations of the window sizes influence the speed of approximation to the adsorption equilibrium, but they have a small influence on the adsorption equilibrium. However, this is true only for cases in which no phase transition of the structure of the MOF happens. Such phase transitions can happen in some cases (see, e.g. 67,68). For the systems which are examined here, such effects have not been observed.

The interactions of Lennard-Jones parameters for the lattice atoms and its partial atomic charges as well as the parameters of CH_4 and H_2S are summarised in the Supporting Material. The GEMC simulations are first equilibrated at target temperatures using 21 runs of 10^8 simulation steps. Further, a run of 10^8 simulation steps is carried out for evaluation.

3. Results and discussion

3.1 Adsorption isotherms and adsorption selectivity

3.1.1 Pure gases

Figure 2 shows the adsorbed amounts of pure gases in several materials at 300 K as a function of the pressure. The adsorbed amount of H_2S is larger than that of CH_4. To obtain an effective separation the difference in the adsorption of the two gases

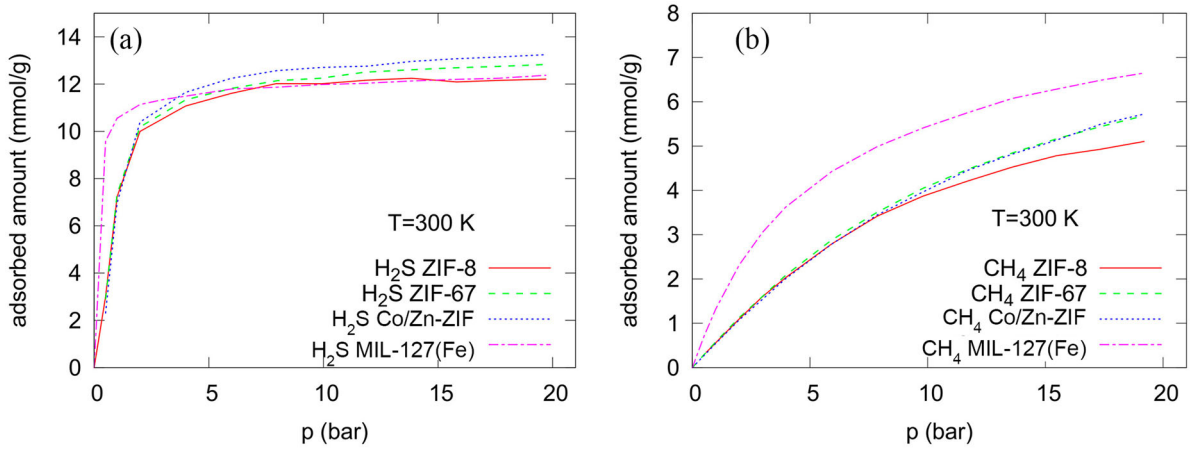

Figure 2. (Colour online) Adsorbed amounts of the pure gases (a) H_2S and (b) CH_4 in several materials at 300 K for various pressures.

should be as large as possible. Up to 10 bar, the adsorption of CH_4 is almost the same for ZIF-8, ZIF-67 and the mixed metal ZIF. That for MIL-127(Fe) is larger. At low pressure, the adsorption of H_2S in MIL-127(Fe) increases more rapidly with increasing pressure than for the other materials. Hence the separation seems to be most effective if MIL-127(Fe) at low pressure is applied. Nonetheless, it will be interesting to see, if this is also true in the case of competitive co-adsorption in the mixture and with the concentration ratio as it is usually found in natural gas.

Figure 3 shows the same at 250 K. As to be expected the adsorption is stronger at the lower temperature. An exception is the adsorption of H_2S, for which saturation is reached at both 250 and 300 K. The temperature dependence of adsorption at low coverage can be described by the Boltzmann factor for adsorption $exp(-U_a/kT)$ where U_a is the absolute value of an effective depth of a potential minimum at an adsorbing surface (see F. Keil [69]).

At 250 K at ambient pressure, particularly the mixed metal ZIF seems to be a promising material for the separation while at pressures below 0.5 bar ZIF-8 and MIL-127(Fe) seem to have a better performance. As mentioned above the separation H_2S/CH_4 must be investigated at realistic concentrations in the mixture before drawing valid conclusions. It turns out that at 250 K the adsorption of H_2S surprisingly quickly reached saturation. The partial pressure of H_2S in the gas phase is 5% of the total pressure in the equilibrium state for all of our simulations. Hence, the sudden saturation of the adsorption within the porous material has nothing to do with the lack of H_2S in the gas phase.

It may be interesting to compare the amount of adsorbed gases from our simulations with experimental values. We found isotherms of different groups of researchers. Note, however, we found that the adsorption of CO_2 in ZIF-8 which measured adsorption isotherms from five different groups showed very different results [70]. The smallest and the largest values differed by a factor of about 2. Hence, such comparisons have to be done with care.

Adsorption isotherms of CH_4 in ZIF-8, ZIF-67 and Co/Zn-ZIF at 273 K up to 1 bar are published [65]. From the graph, we estimate values at 1 bar of about 0.45 mmol/g for ZIF-8, of about 0.54 mmol/g for ZIF-67 and of 0.36 mmol/g for Co/Zn-ZIF. We found in our simulations at 300 K and 1 bar 0.56 mmol/g in ZIF-8, 0.58 mmol/g for ZIF-67 and 0.55 mmol/g for Co/Zn-ZIF. For adsorption isotherms of CH_4 in MIL-127(Fe) at 303 K from 1–10 bar are reported

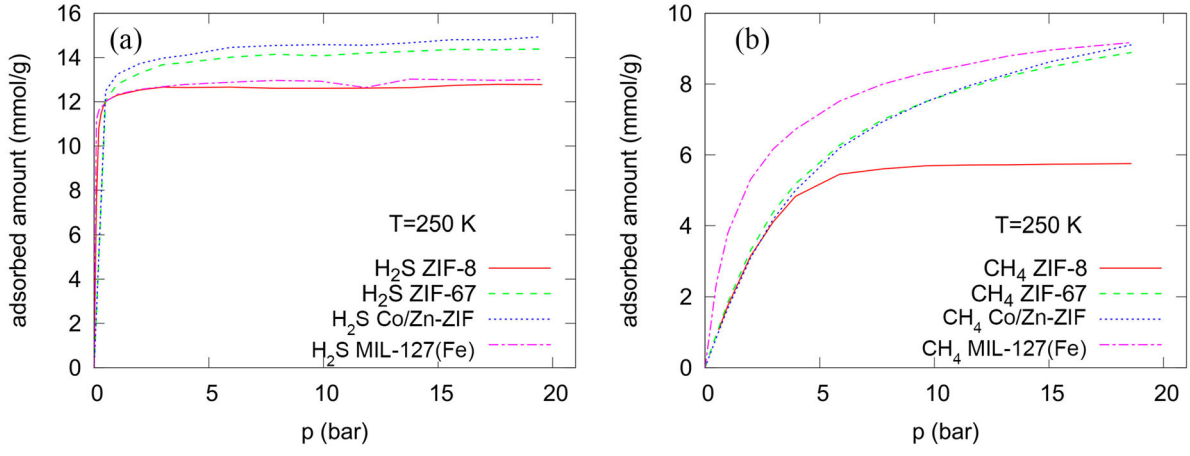

Figure 3. (Colour online) Adsorbed amounts of pure gases (a) H_2S and (b) CH_4 in several materials at 250 K for various pressures.

[71]. From the illustration, the adsorption capacity at 5 and 10 bar are approximately 2.8 and 4.3 mmol/g, respectively. In our simulations at 300 K obtained 4.0 mmol/g for 5 bar and 5.4 mmol/g for 10 bar. The H_2S capacity was investigated for unmodified and modified ZIF-8 at 298 K from 1–10 bar [72]. Unmodified ZIF-8, i.e. DS-ZIF-8 (dry) and WS-ZIF-8 (suspension in methanol) show adsorption capacities at 10 bar about 9 and 18 mmol/g, respectively. This work demonstrated 12.0 mmol/g at 300 K and 10 bar. The adsorption values from simulations are not fitted to experiments. It is quite frequently the case in such comparisons of simulations and experiments. This disagreement can be caused by transport hindrances in real crystals such as lattice defects, grain boundaries, and pore blocking which do not exist in the ideal crystal of the simulations [73] . The adsorption of *e.g.* CH_4 and CO_2 in ZIF-68 and ZIF-69 the hypothesis of partial pore blocking was checked. Blocking some pores randomly is the one choice of blocking obtained a very good agreement of simulations with experiment using unfitted generalised force field parameters.

3.1.2 CH_4/H_2S mixture in ZIF-8

Figure 4(a) shows the amount of the gases, that are adsorbed within the ZIF-8 in equilibrium with the gas phase of the mixture mentioned above. Interestingly at 250 K, the adsorbed amount of CH_4 at $p = 2$ bar is larger than at higher pressures. This is clearly the consequence of competitive co-adsorption because for pure substances at constant temperature the adsorbed amount would be a monotonic function of the pressure. The adsorbed amount of CH_4 at 300 K is larger than that of H_2S as to be expected because in the gas phase (box A) the H_2S content is only 5%. Therefore, also at 300 K, the adsorption selectivity is larger than 1 although more CH_4 than H_2S is adsorbed. This can be seen in Figure 4(b). Interestingly, the selectivity increases with increasing pressure. This is in contrast to the separation of CH_4 from air in ZIF-78 as shown by Channajaree et al. [48]. The selectivity is calculated by Equation (2) where $N_{i,\mathrm{gas}} = N_{\mathrm{CH4},A}$ is the number of CH_4 molecules in box A (gas phase). $N_{j,\mathrm{adsorbed}} = N_{\mathrm{CH4},B}$ is the number of CH_4 molecules in box B (adsorbed phase) and so on. The selectivity increases with increasing pressure.

At 250 K the selectivity as a function of the pressure shows an inflection at about 2–3 bar. For ZIF-8 this inflection is less pronounced than for ZIF-67 and Co/Zn-ZIF. The values for the adsorption selectivity at 1 and 10 bar are given in Supporting Material.

3.1.3 CH_4/H_2S mixture in ZIF-67

Figures 5(a) and (b) show that the adsorption and selectivity for the two gases in ZIF-67 are very similar to the corresponding curves for ZIF-8. The inflection of the selectivity curve at about 2.5 bar is more pronounced for ZIF-67. The reason for a stronger than linear increase of the H_2S adsorption at this pressure is that 'already adsorbed'-H_2S molecules will attract new ones. Note, that the mass of a Zn atom is higher than that of a Co atom. Therefore, an equal amount of adsorbed gas measured in mmol/g corresponds to more adsorbed gas molecules in ZIF-8 as can be seen in Table S5 as shown in the Supporting Material.

3.1.4 CH_4/H_2S mixture in Co/Zn-ZIF

Figures 6(a) and (b) show that the adsorption and selectivity for the two gases in the mixed metal ZIF are slightly different from the corresponding curves for ZIF-8 and ZIF-67. This would agree with the (i) structural component, i.e. metal cluster and organic liker; (ii) structural characteristic, i.e. window aperture, surface area and pore volume. There are no statistical differences between ZIF-8, ZIF-67 and Co/Zn-ZIF as mentioned in Supporting Material.

The adsorption and selectivity for CH_4/H_2S mixture in ZIFs results (Figures 4–6) are lower than MIL-127(Fe) as shown in Figure 7. The explanation is as follows: (i) The structural feature of ZIFs, i.e. ZIF-8, ZIF-67 and Co/Zn-ZIF, that have two types of window aperture such as six-membered ring (~3.4 Å) and four-membered ring (too small). Whereas MIL-127(Fe) has two types of pores such as an accessible one-D channel system around 6 Å and cages of cavity around 10 Å accessible through window apertures of around 4 Å that fit well to the kinetic diameter of CH_4 (3.8 Å) and H_2S (3.6 Å) molecules. (ii) Radial distribution functions (in Section 3.2) and density

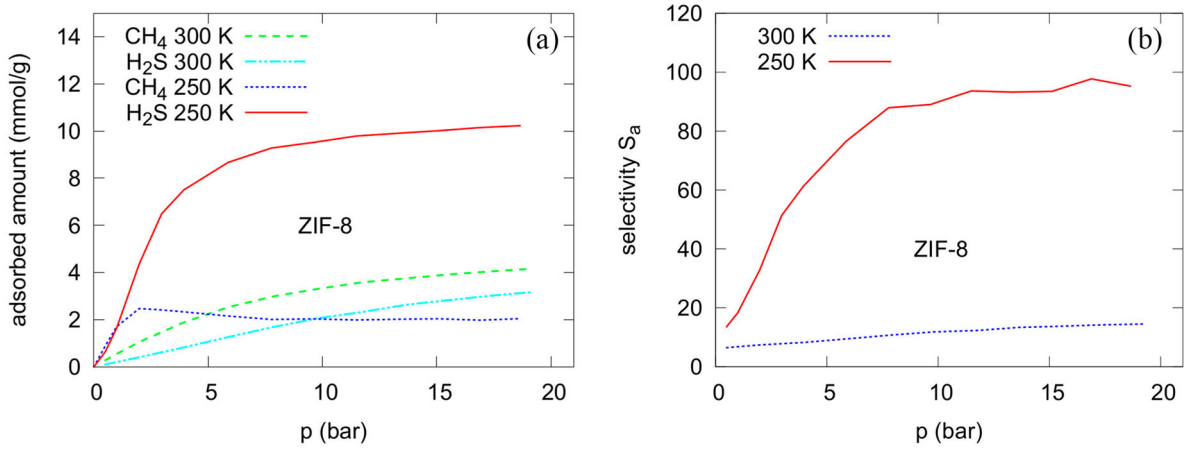

Figure 4. (Colour online) (a) Adsorbed amounts and (b) adsorption selectivity of CH_4 and H_2S in ZIF-8 as a function of the pressure and temperature.

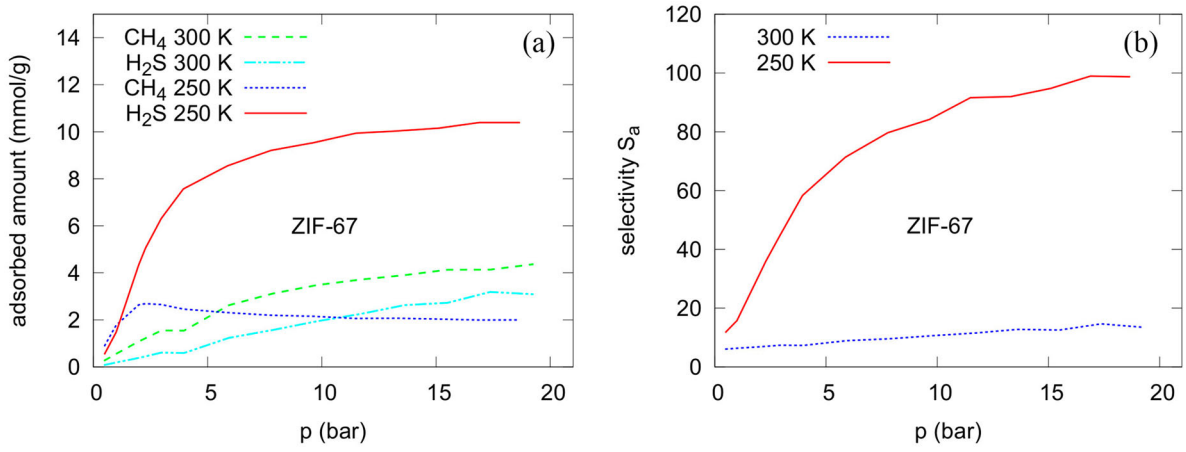

Figure 5. (Colour online) (a) Adsorbed amounts and (b) adsorption selectivity of CH_4 and H_2S in ZIF-67 as a function of the pressure and temperature.

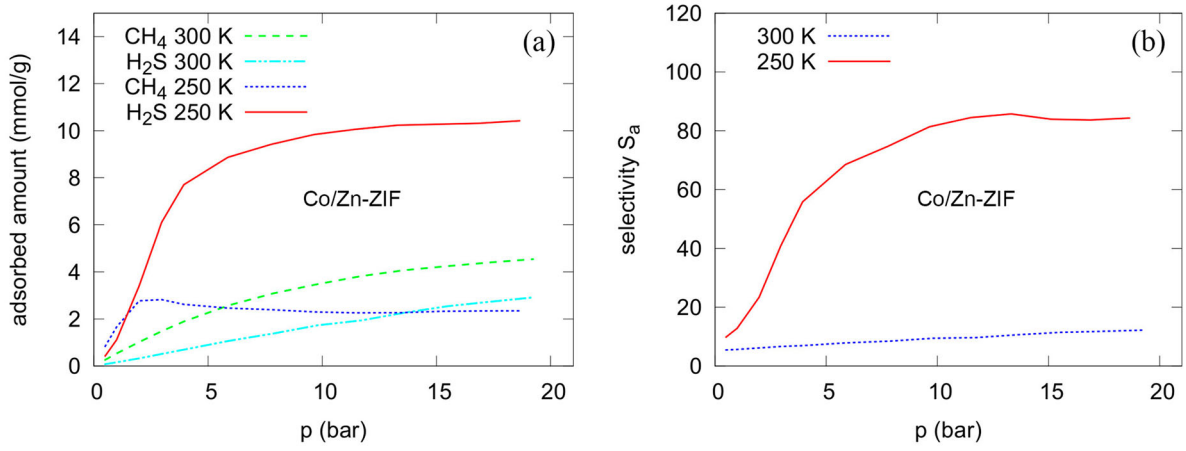

Figure 6. (Colour online) (a) Adsorbed amounts and (b) adsorption selectivity of CH_4 and H_2S in Co/Zn ZIF as a function of the pressure and temperature.

plot (in Supporting Material) show the adsorption site of gas molecules in MIL-127(Fe) including –COO cluster, organic linker and pore channels. However, ZIFs no adsorption site near metal cluster (ZnN_4 o CoN_4 or Co/ZnN_4). (iii) Gas molecule could be adsorbed at organic linker in MIL-127(Fe) easier than ZIFs because of space-size of linker, electronegativity of atom (O = 3.44 and N = 3.04) as confirmed by the enthalpy of adsorption between gas and porous materials in Table 1 and no geometric hindrance effects at O atom in MIL-127(Fe). These reasons are also found in Zho's reported [74].

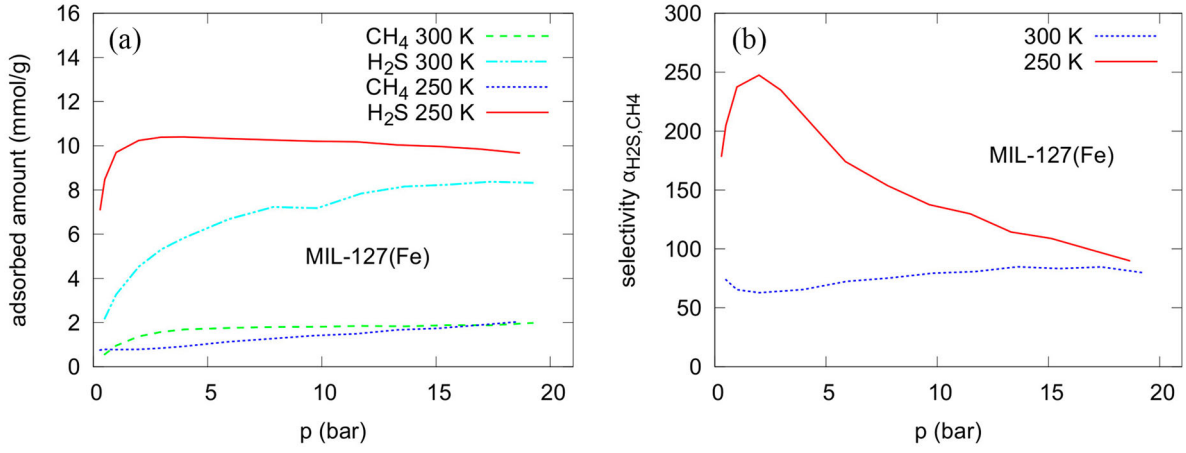

Figure 7. (Colour online) (a) Adsorbed amounts and (b) adsorption selectivity of CH_4 and H_2S in MIL-127(Fe) as a function of the pressure and temperature.

The inflection of the selectivity curve at about 2.5 bar is more pronounced than for ZIF-8. The selectivity at 250 K is about 15% smaller than for ZIF-8 and ZIF-67.

The numbers of guest molecules that are adsorbed in equilibrium in ZIF-67 and the mixed metal ZIF. Like for ZIF-8 at 1 bar about 3 times more CH_4 than H_2S is adsorbed. Note, however, that in the gas phase that is in equilibrium with these adsorbed species, 95% of the particles are CH_4. In Table S5 in the Supporting Material, we compare the numbers of adsorbed particles.

3.1.5 CH_4/H_2S mixture in MIL-127(Fe)

The adsorption and selectivity for CH_4/H_2S mixture in ZIFs results (Figures 4–6) are lower than MIL-127(Fe) as shown in Figure 7. It becomes apparent that the adsorption and selectivity depend on the pore size and window aperture of porous materials. The structural feature of ZIFs, i.e. ZIF-8, ZIF-67 and Co/Zn-ZIF, have two types of window aperture such as 6-membered ring (~3.4 Å) and 4-membered ring (too small). Whereas MIL-127(Fe) has two types of pores such as an accessible 1D channel system around 6 Å and cages of cavity around 10 Å accessible through window apertures of around 4 Å. Therefore, it is the main reason for increasing adsorption and selectivity.

Figure 7(a) shows the amounts of CH_4 and H_2S, that are adsorbed in MIL-127(Fe), as a function of the pressure and temperature. Interestingly, the numbers of adsorbed CH_4 at $T = 250$ K are smaller than at 300 K. It is well known that adsorption is usually stronger at lower temperature and this can be seen in Figure 7 for H_2S. Therefore, the higher selectivity and thus stronger adsorption of H_2S must be the reason for the smaller amount of adsorbed CH_4 at 250 K in MIL-127(Fe). By the way, to avoid artefacts due to the strong adsorption of H_2S and the fact that only 5% of the molecules in the gas phase are H_2S the number of molecules in the gas box must be quite high. A typical run includes about 100 H_2S molecules and 2000 CH_4 molecules in the gas phase in equilibrium.

Figure 7(b) shows the adsorption selectivity of the CH_4/H_2S mixture in MIL-127(Fe) as a function of the pressure. At pressures of 1–3 bar, the selectivity at 250 K can reach values of about 250. That means that with MIL-127(Fe) it is possible to reach high selectivity at low pressures and that this selectivity is higher than for the other materials examined in this paper. Interestingly, the selectivity does not depend monotonically upon the pressure. This fits the fact that H_2S is adsorbed very strongly at low pressure and reaches its saturation value soon, while the adsorption of CH_4 is much smaller but increases monotonically over the whole region of pressure examined here. Although the highest selectivity occurs at 250 K, even at ambient conditions the selectivity of MIL-127 (Fe) is above 50. This may be particularly interesting for industrial applications because it allows separation under ambient conditions.

To get some more insight into the high selectivity at 250 K, it may be of interest to evaluate the enthalpy of adsorption at low pressure for this temperature.

Table 1 shows the enthalpies of adsorption for CH_4 and H_2S at 250 K and at low pressure. The very strong negative enthalpy of adsorption for H_2S, particularly in MIL-127(Fe) illustrates that a high selectivity can be expected.

Table 1. Enthalpy of adsorption in kJ/mol for CH_4 and H_2S at 250 K.

Materials	CH_4	H_2S
ZIF-8	−14.73	−21.76
ZIF-67	−14.73	−21.30
Co/Zn – ZIF	−14.30	−20.15
MIL-127(Fe)	−21.13	−35.36

Note that the potential energy enters the integrand of the classical canonical partition function in the exponent. This integrand is essentially the probability density of a state in phase space. For example, at 2 bar, 250 K (the region of highest selectivity), the average potential energy of an H_2S molecule in MIL-127(Fe) is −33.29 kJ/mol. The potential energy of a CH_4 molecule in the same run is 20.43 kJ/mol. The integrand of the classical canonical partition function is, of course, much more complicated than a simple Boltzmann factor. Nevertheless, the consideration of a Boltzmann factor may give a feeling for the importance of energy differences in the exponent. The Boltzmann factor $\exp\{-U_a/k_BT\}$ changes its value by a factor of 486.29 if $U_a = -33.29$ kJ/mol instead of - 20.43 kJ/mol for $T = 250$ K.

3.2 Radial distribution functions (RDFs)

3.2.1 General remarks

The radial distribution function, RDF, is the probability to find an atom at a radial distance r from a given reference atom. The evaluation of RDFs between atomic pairs of the binary CH_4/H_2S mixtures and the frameworks yields information about optimal gas–gas and gas-framework distances and possible adsorption sites. RDFs within ZIF-8 may be representative also for ZIF-67 and Co/Zn-ZIF that have the same structure. MIL-127(Fe) has a different structure and it is examined separately. More RDF curves are provided in the Supporting Material.

3.2.2 CH_4/H_2S mixture in ZIF-8 at 250 K

Among the three ZIFs with a sodalite crystal structure, ZIF-8 has the best selectivity in the separation of the binary CH_4/H_2S mixtures at all conditions thus it was chosen to represent the structure of each gas inside ZIFs as shown in Figure 8 at 250 K and 1 bar. The C and S labels stand for the atoms C and S, which are the centres of mass of the CH_4 molecule and the H_2S molecule respectively. CC and CT are both C atoms, but at different positions within the lattice, with different chemical bonds to their neighbour atoms and hence different properties.

Three sites of the framework atoms have been considered, Zn of the metal part and CC, CT of the imidazolate part.

The RDFs in Figure 8(a) show that the first maximum of the RDF of the S atom in H_2S with the S atom of another H_2S is somewhat higher than the other two peaks. All of them have the highest maximum at a distance of 4 Å. This is approximately the sum of the two atom radii. But the height of all three peaks is moderate and hence they result only from the kinetic effect that collisions with other molecules are possible only from outside, if two molecules are close to each other.

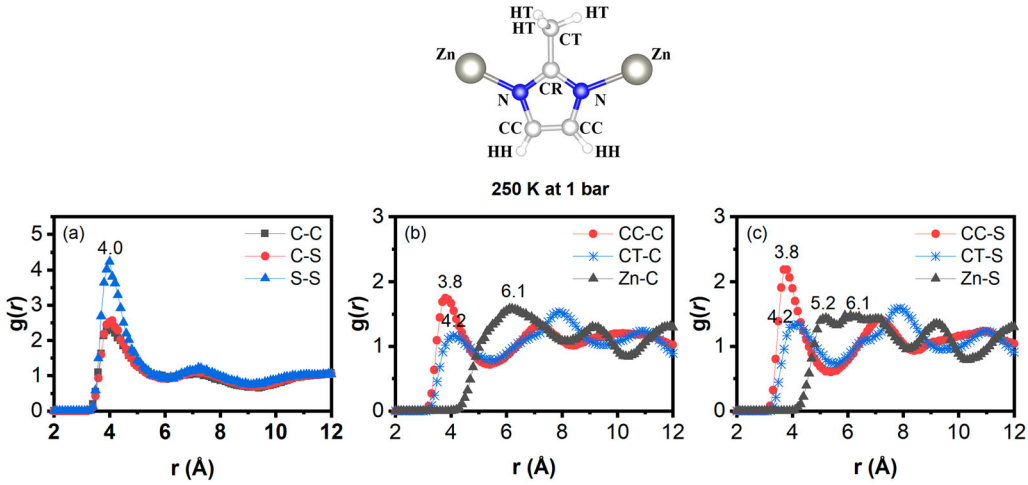

Figure 8. (Colour online) Radial distribution functions (a) between different atoms of the guest molecules, (b) between the C atom in CH_4 with different atoms of the ZIF-8 lattice, that are defined in the inlet picture above, (c) between the S atom of H_2S with these lattice atoms.

Such collisions push the two molecules toward each other. No strong attraction and no clustering can be observed.

Figures 8(b) and (c) show the radial distribution functions of the C and the S atoms with selected lattice atoms. RDFs of the other atoms of the framework with the atoms in guest molecules are available in the Supporting Material.

No remarkable adsorption centres can be observed. Hence the strong adsorption of H_2S results from the low potential energy over larger parts of the pores.

The spatial restrictions make neighbour shells impossible. Therefore, number integrals would not give much useful information.

3.2.3. CH_4/H_2S mixture in MIL-127(Fe) at 250 K

MIL-127(Fe) has the highest selectivity of separation for the binary CH_4/H_2S mixtures at 250 K and about 2 bar. Therefore, the corresponding RDFs are particularly interesting. They can be found in Figure 9. Two regions of the lattice of MIL-127(Fe) at the azobenzenetetracarboxylate (NN and CN) and at the metal cluster (FeO and OD) are examined in Figure 9 while the other RDFs of MIL-127(Fe) with guest atoms can be found in the Supporting Material.

Interestingly, the maximum probability of a close approach between the two C – atoms of different CH_4 is somewhat higher than that of a close approach between two H_2S molecules in MIL-127(Fe) in contrast to ZIF-8. The main difference in the structure of both materials is that the pores of ZIF-8 consist mainly of cavities, connected by bottlenecks, while the pores of MIL-127(Fe) are main channels that form a network. Maybe, the smaller diameter of the channels in comparison to the cavities causes this effect. But the moderate height of all peaks leads to the conclusion that there are no remarkable adsorption centres and hence the low potential energy within the channels and pores is more important for the adsorption than accumulation points of the guest molecules.

4. Conclusion

All porous materials that are investigated in this study (ZIF-8, ZIF-67, Co/Zn-ZIF and MIL-127(Fe)) are suited for separating

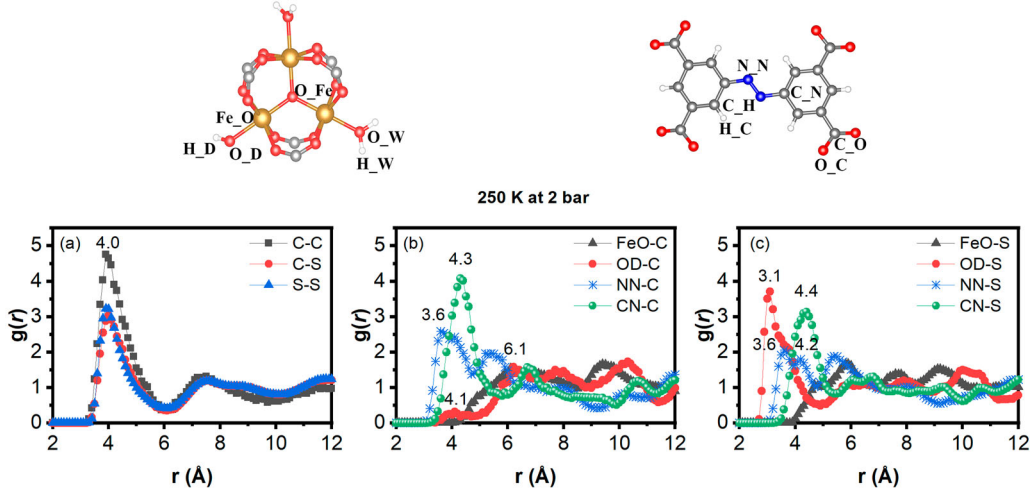

Figure 9. (Colour online) Radial distribution functions (a) between different atoms of the guest molecules, (b) between the C atom in CH_4 with different atoms of the MIL-127(Fe) lattice, that is defined in the inlet picture above, (c) between the S atom of H_2S with these lattice atoms.

H_2S from natural gas but the efficiency is different. For the binary mixture CH_4/H_2S, the H_2S is stronger adsorbed than CH_4 in all materials. Due to the larger channels and pores in MIL-127(Fe) the amount of H_2S that is adsorbed is larger than that in the ZIFs and also the adsorption selectivity is larger. It turned out that MIL-127(Fe) offers also the highest adsorption selectivity. This selectivity reaches its maximum value of 250 at about 2 bar and 250 K. However, even at 300 K the selectivity is between 60 and 80. Therefore, MIL-127(Fe) can be useful for this separation even at room temperature. The other materials considered in this study show very good selectivity of up to nearly 100 at 250 K. For 300 K, their selectivity is much smaller. The selectivity of all materials, considered here, is higher at 250 K than at 300 K. The summarisation can be pointed out that the important key factors for H_2S separation from natural gas in this work not only depend on the potential energy of each gas/material pair but also the structure should have more free space for gas interaction and containing metal oxide for increasing the adsorption site.

Acknowledgements

We thank the Malaysia-Thailand Joint Authority (MTJA) Research Cess Fund (RCF) for financial support. Tanawut Ploymeerusmee would like to acknowledge the Multidisciplinary Program in Petrochemistry and Polymer Science, Faculty of Science, Chulalongkorn University for support.

Disclosure statement

No potential conflict of interest was reported by the author(s).

References

[1] Payne JE. A survey of the electricity consumption-growth literature. Appl Energy. 2010;87(3):723–731.
[2] Zsuzsanna Csereklyei M-V, David IS. Energy and economic growth: the stylized facts. Energy J. 2016;37(Number 2).
[3] Waheed R, Sarwar S, Wei C. The survey of economic growth, energy consumption and carbon emission. Energy Reports. 2019;5:1103–1115.
[4] Liu Y, Wei X, Xiao J, et al. Energy consumption and emission mitigation prediction based on data center traffic and PUE for global data centers. Global Energy Interconnect. 2020;3(3):272–282.
[5] Ahmad T, Zhang D. A critical review of comparative global historical energy consumption and future demand: The story told so far. Energy Reports. 2020;6:1973–1991.
[6] Ajmi AN, Hammoudeh S, Nguyen DK, et al. On the relationships between CO_2 emissions, energy consumption and income: the importance of time variation. Energy Econ. 2015;49:629–638.
[7] Bilgen S. Structure and environmental impact of global energy consumption. Renew Sustain Energy Rev. 2014;38:890–902.
[8] Tahvonen O, Salo S. Economic growth and transitions between renewable and nonrenewable energy resources. European Econ Rev. 2001;45(8):1379–1398.
[9] Praveen RP, Keloth V, Abo-Khalil AG, et al. An insight to the energy policy of GCC countries to meet renewable energy targets of 2030. Energy Policy. 2020;147:111864.
[10] Amri F. Renewable and non-renewable categories of energy consumption and trade: do the development degree and the industrialization degree matter? Energy. 2019;173:374–383.
[11] Shahbaz M, Raghutla C, Chittedi KR, et al. The effect of renewable energy consumption on economic growth: evidence from the renewable energy country attractive index. Energy. 2020;207:118162.
[12] Dogan E, Altinoz B, Madaleno M, et al. The impact of renewable energy consumption to economic growth: a replication and extension of Inglesi-Lotz (2016). Energy Econom. 2020;90:104866.
[13] Adams S, Klobodu EKM, Apio A. Renewable and non-renewable energy, regime type and economic growth. Renew Energy. 2018;125:755–767.
[14] How much carbon dioxide is produced when different fuels are burned? https://www.eia.gov/tools/faqs/faq.php?id=73&t=11.
[15] Busch C, Gimon E. Natural gas versus coal: is natural gas etter for the climate? Electric J. 2014;27(7):97–111.
[16] Saeid Mokhatab WAP. Handbook of natural gas transmission and processing. 2nd ed. Gulf Professional Publishing; 2012.
[17] Faramawy S, Zaki T, Sakr AAE. Natural gas origin, composition, and processing: a review. J Natural Gas Sci Eng. 2016;34:34–54.
[18] Zaman J, Chakma A. Production of hydrogen and sulfur from hydrogen sulfide. Fuel Process Technol. 1995;41(2):159–198.
[19] Gutierrez JP, Benitez LA, Ale Ruiz EL, et al. A sensitivity analysis and a comparison of two simulators performance for the process of natural gas sweetening. J Natural Gas Sci Eng. 2016;31:800–807.
[20] Gabrielli P, Gazzani M, Mazzotti M. On the optimal design of membrane-based gas separation processes. J Membrane Sci. 2017;526:118–130.
[21] Lau CH, Li P, Li F, et al. Reverse-selective polymeric membranes for gas separations. Progr Polymer Sci. 2013;38:740–766.
[22] Liu G, Li N, Miller SJ, et al. Molecularly designed stabilized asymmetric hollow fiber membranes for aggressive natural gas separation. Angew Chem Int Ed. 2016;55(44):13754–13758.
[23] Pandey P, Chauhan RS. Membranes for gas separation. Progr Polymer Sci. 2001;26(6):853–893.
[24] Nurul N, M Z, Jamaliah J SM, et al. Overview of H_2S removal technologies from biogas production. Int J Appl Eng Res. 2016;11(7).
[25] Wu H, Shen M, Chen X, et al. New absorbents for hydrogen sulfide: deep eutectic solvents of tetrabutylammonium bromide/carboxylic acids and choline chloride/carboxylic acids. Sep Purif Technol. 2019;224:281–289.
[26] Song C, Liu Q, Ji N, et al. Natural gas purification by heat pump assisted MEA absorption process. Appl Energy. 2017;204:353–361.
[27] Suleiman B, Abdulkareem AS, Abdulsalam YO, et al. Thermo-economic analysis of natural gas treatment process using triethanolamine (TEA) and diethanolamine (DEA) as gas sweeteners. J Natural Gas Sci Eng. 2016;36:184–201.
[28] Oshima K, Kadonaga R, Shiba M, et al. Adsorption and catalytic decomposition of dimethyl sulfide on H-BEA zeolite. Int J Hydrogen Energy. 2020;45(51):27644–27652.
[29] Haider J, Saeed S, Qyyum MA, et al. Simultaneous capture of acid gases from natural gas adopting ionic liquids: challenges, recent developments, and prospects. Renew Sustain Energy Rev. 2020;123:109771.
[30] Rallapalli PBS, Cho K, Kim SH, et al. Upgrading pipeline-quality natural gas to liquefied-quality via pressure swing adsorption using MIL-101(Cr) as adsorbent to remove CO_2 and H_2S from the gas. Fuel. 2020;281:118985.
[31] Watanabe S. Chemistry of H_2S over the surface of common solid sorbents in industrial natural gas desulfurization. Catalysis Today. 2020.
[32] Lu HT, Kanehashi S, Scholes CA, et al. The impact of ethylene glycol and hydrogen sulphide on the performance of cellulose triacetate membranes in natural gas sweetening. J Membrane Sci. 2017;539:432–440.
[33] Ahmad F, Mukhtar H, Man Z, et al. A theoretical analysis of non-chemical separation of hydrogen sulfide from methane by nanoporous membranes using capillary condensation. Chem Eng Process Process Intensification. 2008;47(12):2203–2208.
[34] Kanehashi S, Aguiar A, Lu HT, et al. Effects of industrial gas impurities on the performance of mixed matrix membranes. J Membrane Sci. 2018;549:686–692.
[35] Hamad F, Qahtani M, Ameen A, et al. Treatment of highly sour natural gas stream by hybrid membrane-amine process: techno-economic study. Sep Purif Technol. 2020;237:116348.

[36] Kárászová M, Vejražka J, Veselý V, et al. A water-swollen thin film composite membrane for effective upgrading of raw biogas by methane. Sep Purif Technol. 2012;89:212–216.
[37] Huang A, Dou W, Caro J. Steam-stable zeolitic imidazolate framework ZIF-90 membrane with hydrogen selectivity through covalent functionalization. J Amer Chem Soc. 2010;132(44):15562–15564.
[38] Hertäg L, Bux H, Caro J, et al. Diffusion of CH_4 and H_2 in ZIF-8. J Membrane Sci. 2011;377(1):36–41.
[39] Samarasinghe SASC, Chuah CY, Yang Y, et al. Tailoring CO_2/CH_4 separation properties of mixed-matrix membranes via combined use of two- and three-dimensional metal-organic frameworks. J Membrane Sci. 2018;557:30–37.
[40] Erucar I, Keskin S. High-throughput molecular simulations of metal organic frameworks for CO_2 separation: opportunities and challenges. 2018;5(4).
[41] Li J-R, Sculley J, Zhou H-C. Metal–organic frameworks for separations. Chem Rev. 2012;112(2):869–932.
[42] Fritzsche S, Chokbunpiam T, Caro J, et al. Combined adsorption and reaction in the ternary mixture N_2, N_2O_4, NO_2 on MIL-127 examined by computer simulations. ACS Omega. 2020;5(22):13023–13033.
[43] Wang S, Wu D, Huang H, et al. Separation science and engineering. Chinese J Chem Eng. 2015;23(8):1291–1299.
[44] Sheikh Alivand M, Hossein Tehrani NHM, Shafiei-alavijeh M, et al. Synthesis of a modified HF-free MIL-101(Cr) nanoadsorbent with enhanced H_2S/CH_4, CO_2/CH_4, and CO_2/N_2 selectivity. J Environ Chem Eng. 2019;7(2):102946.
[45] Sokhanvaran V, Gomar M, Yeganegi S. H_2s separation from biogas by adsorption on functionalized MIL-47-X (X = −OH and −OCH_3): A simulation study. Appl Surf Sci. 2019;479:1006–1013.
[46] Maghsoudi H, Soltanieh M. Simultaneous separation of H_2S and CO_2 from CH_4 by a high silica CHA-type zeolite membrane. J Membrane Sci. 2014;470:159–165.
[47] Heck HH, Hall ML, dos Santos R, et al. Pressure swing adsorption separation of H2S/CO2/CH4 gas mixtures with molecular sieves 4A, 5A, and 13X. Sep Sci Technol. 2018;53(10):1490–1497.
[48] Chanajaree R, Chokbunpiam T, Kärger J, et al. Investigating adsorption- and diffusion selectivity of CO_2 and CH_4 from air on zeolitic imidazolate framework-78 using molecular simulations. Micro Meso Mater. 2019;274:266–276.
[49] Chokbunpiam T, Chanajaree R, Caro J, et al. Separation of nitrogen dioxide from the gas mixture with nitrogen by use of ZIF materials; computer simulation studies. Comput Mater Sci. 2019;168:246–252.
[50] Schierz P, Fritzsche S, Janke W, et al. MD simulations of hydrogen diffusion in ZIF-11 with a force field fitted to experimental adsorption data. Micro Meso Mater. 2015;203:132–138.
[51] Chokbunpiam T, Fritzsche S, Caro J, et al. Importance of ZIF-90 lattice flexibility on diffusion, permeation, and lattice structure for an adsorbed H_2/CH_4 gas mixture: a re-examination by Gibbs ensemble monte carlo and molecular dynamics simulations. J Phys Chem C. 2017;121(19):10455–10462.
[52] Pongsajanukul P, Parasuk V, Fritzsche S, et al. Theoretical study of carbon dioxide adsorption and diffusion in MIL-127(Fe) metal organic framework. Chem Phys. 2017;491:118–125.
[53] Chokbunpiam T, Fritzsche S, Parasuk V, et al. Molecular simulations of a CO_2/CO mixture in MIL-127. Chem Phys Lett. 2018;696:86–91.
[54] Panagiotopoulos AZ, Quirke N, Stapleton M, et al. Phase equilibria by simulation in the Gibbs ensemble. Mol Phys. 1988;63(4):527–545.
[55] Daan Frenkel BS. Understanding molecular simulation. 2 nd ed. Academic Press; 2001.
[56] Theodorou DN. Progress and outlook in Monte Carlo simulations. Ind Eng Chem Res. 2010;49(7):3047–3058.
[57] Dubbeldam D, Torres-Knoop A, Walton KS. On the inner workings of monte carlo codes. Mol Simul. 2013;39(14–15):1253–1292.
[58] Peng D-Y, R DB. A new two-constant equation of state. Ind Eng Chem Fund. 1976;15(1):6.
[59] Rull LF, Jackson G, Smit B. The condition of microscopic reversibility in Gibbs ensemble Monte Carlo simulations of phase equilibria. Mol Phys. 1995;85(3):435–447.
[60] June RL, Bell AT, Theodorou DN. Prediction of low occupancy sorption of alkanes in silicalite. J Phys Chem. 1990;94(4):1508–1516.
[61] Myers AL. Thermodynamics of adsorption. In: Letcher T, editor. Chemical thermodynamics for industry. X: The Royal Society of Chemistry; 2004. p. 243–253.
[62] Siažik J, Malcho M. Accumulation of primary energy into natural gas hydrates. Proc Eng. 2017;192:782–787.
[63] Park KS, Ni Z, Côté AP, et al. Exceptional chemical and thermal stability of zeolitic imidazolate frameworks. Proc Natl Acad Sci. 2006;103(27):10186.
[64] Hayashi H, Côté AP, Furukawa H, et al. Zeolite A imidazolate frameworks. Nature Mater. 2007;6(7):501–506.
[65] Zhou K, Mousavi B, Luo Z, et al. Characterization and properties of Zn/Co zeolitic imidazolate frameworks vs. ZIF-8 and ZIF-67. J Mater Chem A. 2017;5(3):952–957.
[66] Wongsakulphasatch S, Nouar F, Rodriguez J, et al. Direct accessibility of mixed-metal (iii/ii) acid sites through the rational synthesis of porous metal carboxylates. Chem Commun. 2015;51(50):10194–10197.
[67] Gücüyener C, van den Bergh J, Gascon J, et al. Ethane/ethene separation turned on its head: selective ethane adsorption on the metal−organic framework ZIF-7 through a gate-opening mechanism. J Amer Chem Soc. 2010;132(50):17704–17706.
[68] Aguado S, Bergeret G, Titus MP, et al. Guest-induced gate-opening of a zeolite imidazolate framework. New J Chem. 2011;35(3):546–550.
[69] Keil F. Diffusion and chemische reaktionen in der Gas/Feststoff-Katalyse. 1 ed. Berlin, Heidelberg: Springer; 1999.
[70] Chokbunpiam T, Fritzsche S, Chmelik C, et al. Gate opening effect for carbon dioxide in ZIF-8 by molecular dynamics – confirmed, but at high CO_2 pressure. Chem Phys Lett. 2016;648:178–181.
[71] Chanut N, Wiersum AD, Lee UH, et al. Observing the effects of shaping on gas adsorption in metal-organic frameworks. Eur J Inorganic Chem. 2016;27:4416–4423.
[72] Jameh AA, Mohammadi T, Bakhtiari O, et al. Synthesis and modification of zeolitic imidazolate framework (ZIF-8) nanoparticles as highly efficient adsorbent for H_2S and CO_2 removal from natural gas. J Environ Chem Eng. 2019;7(3):103058.
[73] Babarao R, Dai S, Jiang D-e. Effect of pore topology and accessibility on gas adsorption capacity in zeolitic−imidazolate frameworks: bringing molecular simulation close to experiment. J Phys Chem C. 2011;115(16):8126–8135.
[74] Zhou M, Wang Q, Zhang L, et al. Adsorption sites of hydrogen in zeolitic imidazolate frameworks. J Phys Chem B. 2009;113(32):11049–11053.